particle analyzer was used to monitor changes in particle sizes. A conventional ESP placed at the outlet of the agglomeration chamber was used to collect particles. This experiment investigated the effect of using a coupling field compared with a single field, in terms of median particle diameter change and removal efficiency.

EXPERIMENTAL SETUP AND METHODOLOGY

In this experiment, the feeding system comprised a SAG 410/L aerosol generator, with a flow rate of 1–264 g h^{-1} (Fig. 1). The agglomeration chamber was a vertical cuboid fabricated from polymethyl methacrylate (PMMA). The height of the chamber was 1200 mm, and the side length was 120 mm. Inside the chamber, four stainless steel wire electrodes were located every 100 mm and each had a diameter of 2 mm and a length of 80 mm. Additionally, the chamber contained two discharge plates for the production of pulse corona discharges. Sound-absorbing foam was used in the chamber to reduce the reflection of sound waves. The acoustic wave system comprised a SFG-1013 signal generator, YF-513 compression driver, and a QSC RMX2450 power amplifier, which were used to set acoustic frequencies between 180 and 5500 Hz. Based on the consideration that energy input breaks aggregates into pieces, SPLs between 135 and 143 dB were chosen in this study. These SPLs have been proven effective in other studies (Liu *et al.*, 2009; Wang *et al*., 2011). The pulsed corona discharge system involved a narrow-pulse HV generator, Tektronix TCP0150 current probe, Tektronix DPO4034 digital oscilloscope, and P150-GL HV probe. The system was used to control input parameters and acquire the I-V curve.

Subsequently, particles flowed through the agglomeration chamber, and particle size distribution (PSD_1) was captured using a DP-02 laser particle size analyzer. An electrical low pressure impactor (ELPI) was placed after the ESP to measure the particle concentration and particle size distribution between 0 and 10 μm (PSD_2). A two-stage diluter was used to ensure that the flow rate to the ELPI was 10 m^3 h^{-1}. The ESP was wire-plated and used a negative direct current (DC) power supply.

Jiaxing coal-fired plant fly ash particles were used in this experiment, and they were mixed before being released into the agglomeration chamber. A DP-02 laser particle size analyzer was used to ensure that a laser beam could penetrate the bottom part of the agglomeration chamber. In this study, the ELPI measurement range was less than10 μm, but a substantial proportion of the agglomerated particles was larger than 10 μm. The DP-02 laser particle size analyzer was utilized to measure the size change of the agglomerated particles to verify the effect of the coupling field.

THEORETICAL ANALYSIS

Particle charges, particle collisions, and particle–gas interactions are involved in the processes of particle agglomeration and removal. Thus, when particles flow through an agglomeration chamber, multiple forces may act upon them, such as Coulomb force between charged particles, viscous Stokes' drag force, gravitational force, inertial force, and buoyancy force. The mechanism resulting from these mutually influential forces is complex.

Pulse Corona Discharge

High-voltage pulse discharge differed from negative DC discharge; the high-voltage discharge process comprised two stages: a discharge period and an intercritical period. In this study, high-voltage generator frequency ranged from 100 to 300 Hz, but the pulse width was only 300–400 ns, and the intercritical period was much longer than the discharge period. Discharge occurred in formed streamer-channels in which numerous high-energy free electrons and ions coexisted. The high-energy free electrons migrated more rapidly than did the ions, and in the agglomeration chamber, the concentrations of positive and negative ions were extremely unbalanced (McAdams, 2007). Thus, the discharge period, mainly involved the charging of fine particles by high-energy free electrons. After the discharge period, numerous ions remained in the reaction space. The number of negative ions was substantially lower than that of positive ions, and most of the negative ions were neutralized within a short period (McAdams, 2007). Thus, charges from positive ions were more prevalent on fine particles.

Based on the preceding analysis, during the discharge period, electron flux was solved to identify charge number (Liu and Kapadia, 1978; O'Hara *et al*., 1989):

$$\Pi\big|_r = -\mu_e N_e(r) E - D_e \nabla N_e(r) \tag{1}$$

where μ_e is the migration rate of high-energy free electrons; $N_e(r)$ is the concentration of high-energy free electrons r away from the particle center; D_e is the diffusion coefficient of high-energy free electrons; and $\nabla N_e(r)$ is the concentration gradient of high-energy free

electrons r away from the particle center.

When electron flux is small, Einstein's equations should be introduced to solve Eq. (1), where the energy distribution of high-energy free electrons is assumed to conform to Maxwell distribution (Bates *et al.*, 1962):

$$KT_e = \frac{2}{3} X (\frac{D_e}{\mu_e}) e \tag{2}$$

where K is the Boltzmann constant; K = 1.38×10^{-23} J K^{-1}; T_e is the temperature of high-energy free electrons; X is a constant; and X = 3/2 when energy distribution of high-energy free electrons conforms to Maxwell distribution,

$$\ln N_{e(r)} = \frac{e\Phi_{(r)}}{KT_e} + A \tag{3}$$

Where $\Phi_{(r)}$ is electric potential r away from the particle center; A is a constant; and the boundary conditions are $\Phi_{(r)} = 0$, $N_{e(r)} = N_{e0}$,

$$N_{e(r)} = N_{e0} \exp(\frac{-e\Phi_{(r)}}{KT_e}) \tag{4}$$

where N_{e0} is the original concentration of high-energy free electrons. If electron flux is large enough or the ratio of electric field intensity to gas molecular density is large enough, the energy

distribution of high-energy free electrons deviates from Maxwell distribution; Eq. (4) is no longer applicable; and $\Phi_{(r)}$ refers to electric potential under the influence of particles' own charge and external electric field,

$$\Phi_{(r)} = \frac{-q_1}{4\pi\varepsilon_0 r} - [\frac{r}{R} - (\frac{\varepsilon - \varepsilon_0}{\varepsilon + 2\varepsilon_0})\frac{R^2}{r^2}]E_0 a\cos\theta \qquad (r \geq R) \tag{5}$$

where q_1 is particle charge; r is the distance between a point in the reaction system and a particle center; ε is a particle's relative dielectric constant; ε_0 is the permittivity of vacuum; E_0 is the original electric field intensity in the reaction system; θ is the angle of a line between the particle center and a point r away from the particle center and the electric field line.

Eqs. (1, 4, 5) indicate that high-energy free electron flux could be created on the surface of particles,

$$\frac{\mathrm{d}q_1}{\mathrm{d}t} = -2\pi e a^2 \int_{\theta=0}^{\theta=\pi} \Pi|_{r=a} \sin\theta \mathrm{d}\theta \tag{6}$$

To solve Eq. (6), the boundary condition ($\nabla N_e(r=R)=0$) should be applied, because electron density distribution conforms to Boltzmann distribution, and continuous electron distribution occurs around particles. Thus, solution is as follows:

$$q_1 = \frac{4\pi\varepsilon_0 RKT_e}{e}\ln[1 + \frac{N_{e0}Re^2\mu_e E_0 t}{2\varepsilon_0 KT_e}(\frac{e^{\alpha} - e^{-\alpha}}{\alpha})] \tag{7}$$

$$\alpha = \frac{-3eE_0R}{(\frac{\varepsilon}{\varepsilon_0}+2)KT_e} \tag{8}$$

With the increase of electric field intensity, particles receive more charges. Similarly, after the discharge period, particles capture positive ions and become positively charged:

$$q_2 = \frac{4\pi\varepsilon_0 RKT}{e} \cdot \ln[1+\exp(-\frac{e^2B}{RKT})\frac{\pi u_i e^2 RN_{i0}t}{KT}] \tag{9}$$

where B is a constant related to R, ε, and ε_0.

Due to the opposite charges present among particles during the discharge period, Coulomb force exists in the agglomeration chamber:

$$F_C = \frac{q_1 q_2}{4\pi\varepsilon R^2} \tag{10}$$

According to studies on fine particle charges (Jiang *et al.*, 2015; Xu *et al.,* 2009), small and large particles exhibit opposite charges and attract each other, resulting in the formation of numerous aggregates.

Acoustic Wave Field

Acoustic wave is a promising pretreatment method for achieving particle agglomeration. In an intensive acoustic wave field, particles are entrained by gas media. Orthokinetic interaction plays

196 a key role in the acoustic agglomeration process (Sheng and Shen, 2007). In the orthokinetic
197 interaction process, an acoustic wave causes air medium vibration; because of the viscosity of the
198 gas, particles in the aerosol vibrate in response. Large particles with large inertia are not readily
199 carried by gas while small particles are easy to be carried. Different vibration amplitudes result in
200 relative motion and collision between particles of different sizes, and the entrainment coefficient
201 μ_p can be defined as follows (Zhou *et al*., 2017):
202
203 $$\mu_p = \frac{u_p}{u_g} \tag{11}$$
204
205 Several forces are present in the acoustic field, namely pressure gradient force, viscous Stokes'
206 drag force, and the force required for fluid acceleration near the particles. In this study, particle
207 motion was limited within Stokes flow (Re < 1), and only viscous Stokes' drag force was
208 considered:
209
210 $$F_p = \frac{6\pi\mu_g R(u_g - u_p)}{c_c} \tag{12}$$
211
212 where μ_g is the dynamic viscosity of gas; R is particle radius; u_g is the velocity of gas; u_p is the
213 velocity of particles; and C_c is Cunningham correction factor (Fan *et al*., 2013).
214 Entrained particles in gas medium vibrate and lag behind the gas. The particle motion equation
215 can be expressed as follows:

$$u_g = u_0 \sin \omega t \tag{13}$$

The velocity of particles can then be simplified as follows,

$$u_p = \frac{u_0 \sin(\omega t - \varphi)}{\sqrt{1 + \omega^2 \tau^2}} \tag{14}$$

where τ is the relaxation time of particles, u_0 is the velocity amplitude of gas medium; ω is angular frequency; and $\omega=2\pi f$,

$$\tau = \frac{2\rho R^2 C_c}{9\mu_g} \tag{15}$$

Where f is the acoustic wave frequency. φ is the phase difference between gas medium and particles, so the entrainment coefficient μ_p can be de represented as follows:

$$\mu_p = \frac{1}{\sqrt{1 + \omega^2 \tau^2}} = \frac{1}{\sqrt{1 + 4\pi^2 f^2 \tau^2}} = \cos \varphi \tag{16}$$

Fig. 2 presents the effects of particle size and acoustic wave frequency on the acoustic entrainment factor. The value of μ_p is between 0 and 1, and a larger entrainment factor signifies that particles are readily entrained by the gas medium. When μ_p reaches 1, the vibration

amplitude of the particles and air medium is synchronized. By contrast, when μ_p is 0, particle motion is not affected by acoustic waves and remains vibrationless. Larger particles are easily entrained when acoustic wave frequency is low. Specific frequencies, correspond with specific entrainment factors. These factors can be utilized to prove the existence of optimal acoustic parameters for inducing relative movement and collision of particles with various diameters.

In the acoustic wave field, countless particles collide, and large particles are likely to be shattered by acoustic waves. Because of the existence of a pulse corona field, particles with various diameters receive opposite charges due to differences in charging mechanisms, and Coulomb force may cause them to adhere and aggregate into larger particles. Thus, the coupling effect increases the possibility of reunion and agglomeration. Application of ESP substantially increases the efficiency of small particle removal.

RESULTS AND DISCUSSION

In this study, fly ash particle was assumed to be a convex spherical particle. A DP-02 laser particle analyzer and ELPI were utilized to measure the particle agglomeration process and particle removal efficiency respectively. Studies have focused on measuring removal efficiency using ELPI. ELPI measurement range is less than 10 μm; thus, ELPI is insufficient for monitoring particles with larger diameters. In this study, DP-02 was selected to measure particle size change online. The particle size measuring mechanisms of ELPI and the DP-02 laser particle analyzer differ; ELPI data are based on aerodynamic size, whereas DP-02 data are based on

257 optical particle size. As presented in Fig. 3, original particle size distribution PSD_1 (DP-02) was
258 compared with transformed PSD_2 (ELPI) in the same coordinate system. The results show that the
259 curves of the PSDs coincided; thus, the respective PSDs could be used to investigate
260 agglomeration and removal efficiency.

261 In a DC electric field, I–V characteristic curve was used to analyze the power supply properties.
262 A narrow-pulse HV generator was used as an intermittent discharge device. Consideration of
263 energy input was required. Energy input reflects electron and ion density changes and reaction
264 processes, as well as migration rate. Single pulse energy was introduced to describe pulsed
265 corona discharge energy consumption. Pulse corona discharge frequency ranged from 100 to 300
266 Hz. Fig. 4 illustrates the pulsed corona discharge characteristics. When input voltage increased,
267 single pulse energy will increased; in other words, more energy was injected into the reaction
268 space, and 100 Hz single pulse energy was the largest, followed by 200 and 300 Hz.

269

270 ***Effects of Pulse Corona Discharge on the Agglomeration of Fine Particles***

271 The purpose of this experiment was to verify the influence of pulse corona discharge on PSD_1.
272 The results are as presented in Fig. 5(a). New peak values in the pulse field were noted, and the
273 corresponding median particle size increased. When the voltage was 35 and 45 kV, the new peak
274 value after agglomeration was approximately 30 μm, and the volume proportions of 27-μm
275 particles reached 4.46% and 11.84%, respectively. Most small particles remained. When the pulse
276 voltage increased to 55 kV, the volume proportion of small particles dramatically decreased. The
277 proportion of 9.82-μm particles dropped to 31.28%, and the proportion of 27-μm particles

increased to 25.96%. When the pulse frequency was 100 or 200 Hz, new peaks appeared at 155 μm, and the peak values were 6.29% and 4.01%, respectively. Fig. 5(b) illustrates that in the pulse corona discharge field, the median particle size after agglomeration clearly increased. As input voltage increased and pulse frequency decreased, D_{50} increased, reaching 23 μm under the condition of 55 kV-100 Hz. Energy input ionized the air and the concentration of high-energy free electrons and ions increased dramatically, which may have increased the intensity of mutual force between charged particles, resulting in easier aggregation of particles.

Agglomeration ratio (R_{ae}) was defined as the ratio of the median particle size after agglomeration to the median size of the original particles. As presented in Fig. 6, when the input voltage was 55 kV, the pulse frequency was 100 Hz; the corresponding median diameter was 23.39 μm; and R_{ae} was 2.93. When the input voltage was increased from 35 to 45 kV, D_{50} and R_{ae} did not exhibit significant changes. This finding suggested that large pulse voltage and low pulse frequency should be selected to maximize the effectiveness of agglomeration within the limits of the experimental conditions.

Effects of Acoustic Wave on the Agglomeration of Fine Particles

In these experiments, because of limits in the experimental conditions, SPLs were 135, 139, and 143 dB. As denoted in Table 1, when SPL was 143dB, both the D_{50} and R_{ae} both first increased and then decreased as the acoustic wave frequency increased. With the decrease of SPL, D_{50} and R_{ae} also decreased. Therefore, the larger the SPL is, the more intense the particle vibration. Additionally, the probability of collision between particles increased and the optimum

299 acoustic frequency was 1600 Hz.

300 Experiments were performed to investigate the effects of acoustic waves on the agglomeration
301 of fine particles. According to the results of the previously described experiments, SPL = 143 dB
302 was selected. As Fig. 7 presents, the effect of the acoustic frequency on the aggregation of fine
303 particles was complex. When acoustic frequency was 2400 Hz, a new small peak value appeard
304 between 20 and 30 μm. The effects of 800 and 1200 Hz were similar: a wide range of peaks
305 appeared; almost all fine particles agglomerated into large particles; and most particles were 20 –
306 80 μm. The frequency of 1600 Hz was most effective for agglomeration; not only did the small
307 particles all agglomerate into large particles but also the peak value was larger than 40 μm after
308 agglomeration. Additionally, obvious peaks were evident at 200 μm. when SPL was 143 dB, the
309 acoustic frequency was 1600 Hz; D_{50} of fine particles changed from 7.98 to 57.56 μm, and R_{ae}
310 reached 7.21 (Fig. 8). By contrast, when acoustic frequency was 2400 Hz, D_{50} was only 20.52 μm,
311 and the corresponding R_{ae} was only 2.57. The findings suggested that acoustic frequency should
312 neither be too large nor too small and that optimal frequency value was 1600Hz. Orthokinetic
313 interaction was the predominant mechanism, suggesting that relative movement and collision
314 resulted from differences in the entrainment degrees of particles. If the acoustic frequency was
315 too small, all particles vibrated with the gas medium, and relative motion among particles with
316 different sizes was small. If the acoustic wave frequency was too large, all particles remained still
317 and could not vibrate with the gas medium, and a relative motion effect was not obvious.
318 Therefore, selection of an appropriate acoustic frequency was crucial for ensuring an optimal
319 fine particle agglomeration effect.

320

321 ***Effect of Coupling Field on the Agglomeration of Fine Particles***

322 This experiment was conducted in the acoustic wave and pulse discharge coupling field. The
323 results are presented in Fig. 9. The pulse frequency and voltage were 100 Hz and 55 Kv,
324 respectively, and the acoustic frequency and SPL were 1600 Hz and 143 dB, respectively. The
325 volume proportion of large particles obviously increased, whereas that of fine particles decreased
326 substantially. Most particles with diameters of 9.82 μm were agglomerated into larger particles.
327 The volume proportion of particles with a diameter of 200.68 μm increased to 16.98% in the
328 coupling field and to 1.93% in the pulse corona discharge field. As denoted in Fig. 9(b), D_{50} and
329 R_{ae} significantly increased in the coupling field compared with the single field, reaching 73.28
330 μm and 9.18, respectively. Thus, the efficiency of fine particle agglomeration in the coupling field
331 was greater than that of the single field, and D_{50} increased considerably.

332

333 ***Particle Removal Efficiency in Coupling Field***

334 To determine whether agglomeration in the coupling fieldincreased removal efficiency, a
335 laboratory-scale ESP with a negative DC supply was placed at an outlet of the agglomeration
336 chamber. Studies have proven that a negative DC can remove particles efficiently, with the
337 exception of fine particles. In this study, acoustic wave and pulse corona discharge coupling field
338 were used as a pretreatment to force fine particles to agglomerate into larger particles, resulting in
339 significantly more efficient fine particle removal. Removal efficiency was calculated using Eq.
340 (17):

$$\eta = 1 - \frac{N}{N_0} \tag{17}$$

where N_0 is the initial particle number concentration (PNC), and N is PNC at the outlet of the ESP. In this study, the parameters were the same as those used in the previously described agglomeration experiment. DC supply voltage was regulated to 16 kV, which was the highest voltage applied to the ESP in this experiment. As shown in Fig. 10, PNC clearly decreased after particles passed through the ESP. Additionally, the amplitude of PNC decreased less for particles with diameters of 0.15 μm than for those of other sizes. As Fig. 11 illustrates, ESP removal efficiency significantly increased with pretreatment, especially in the coupling field. When only DC supply was applied, removal efficiency was 80.7%, and that of particles with diameters of 0.15 μm was less than 75%.

When particles passed through the agglomeration chamber first, fine particles removal efficiency increased sharply. When the pretreatment was pulse corona discharge, the efficiency increased to approximately 91.6%, and when an acoustic wave field was applied, removal efficiency further increased to 94.4%. Particles with diameters of 0.15 μm were present in the critical area of field charge and diffusion charge; although these particles were difficult to remove, pretreatment resulted in considerable increases in the efficiency of their removal from 75% to 80%, 85%, and 91%. Additionally, overall particle removal efficiency reached 98.3%.

CONCLUSIONS

Comparative experimental studies were conducted to verify the effects of pulse corona discharge and acoustic wave coupling on particle agglomeration and removal efficiency. The coupling field clearly increased agglomeration efficiency when the pulse corona discharge and acoustic wave parameters were 55 kV-100 Hz and 143 dB-1600 Hz, respectively, and D_{50} and R_{ae} values were 11.23 μm, 1.51 and 57.56 μm, 7.21. In the coupling field, the corresponding values increased to 73.28 μm and 9.18, and the effect on agglomeration was obvious. The acoustic wave value of 1600 Hz was optimal for enhancing the agglomeration effect, and when the SPL value rose, agglomeration efficiency increased in response. When pulse frequency was 100 Hz, the single pulse energy injection reached its maximum, and more fine particles were charged and aggregated into larger particles. Under the acoustic wave and pulse corona discharge coupling field, overall removal efficiency reached 98.3%, and particles with diameters of 0.15 μm were in the critical area of field charge and diffusion charge. Although these particles were difficult to remove, the grade removal efficiency substantially improved, from 75.1% to 80%, 85.3%, and 91.4%. Finally, the coupling field was more effective than the single field as a pretreatment for fine particle.

ACKNOWLEDGEMENTS

This work was supported from the National Basic Research Program (973) of China (No. 2013CB228504). This manuscript was edited by Wallace Academic Editing.

REFERENCES

Bates, D.R., Massey, H.S.W. and Amdur, I. (1962). Atomic and molecular processes. *Phys. Today*. 15: 63-63.

Chen, C.C., Tao, C.J. and Cheng, H.C. (2002). Condensation of supersaturated water vapor on charged/neutral nanoparticles of glucose and monosodium glutamate. *J. Colloid Interface Sci.* 255: 158-170.

Chen, H., Wang, T., Luo, Z., Zhou, D., Lu, M., He, M., Fang, M. and Cen, K. (2017). Agglomeration kernel of bipolar charged particles in the presence of external acoustic and electric fields. *Aerosol Air Qual. Res*. 17: 857-866.

Fan, F., Yang, X. and Chang, N.K. (2013). Direct simulation of inhalable particle motion and collision in a standing wave field. *J. Mech. Sci. Technol.* 27: 1707-1712.

Hoffmann, T.L. (2000). Environmental implications of acoustic aerosol agglomeration. *Ultrasonics.* 38: 353.

Jiang, J.P., Luo, Z.Y., Chen, H., Zhou, D., Sha, D.H., Fang, M.X. and Cen, K.F. (2015). Orthogonal design process optimization for particle charge distribution of mosquito coil smoke aerosol enhanced by pulsed corona discharge. *Powder Technol.* 286: 507-515.

Le, T.C., Lin, G.Y. and Tsai, C.J. (2013). The Predictive Method for the Submicron and Nano-Sized Particle Collection Efficiency of Multipoint-to-Plane Electrostatic Precipitators. *Aerosol Air Qual. Res*. 13: 1404–1410.

Liao, Z., Li, Y., Xiao, X., Wang, C., Cao, S. and Yang, Y. (2018). Electrostatic precipitation of submicron particles with an enhanced unipolar pre-charger. *Aerosol Air Qual. Res*. 18.

Liu, B.Y.H. and Kapadia, A. (1978). Combined field and diffusion charging of aerosol particles in the continuum regime. *J. Aerosol Sci.* 9: 227-242.

Liu, J., Wang, J., Zhang, G., Zhou, J. and Cen, K. (2011). Frequency comparative study of coal-fired fly ash acoustic agglomeration. *Res. J. Environ. Sci.* 23: 1845-1851.

Liu, J., Zhang, G., Zhou, J., Wang, J., Zhao, W. and Cen, K. (2009). Experimental study of acoustic agglomeration of coal-fired fly ash particles at low frequencies. *Powder Technol.* 193: 20-25.

Liu, J.X., Gao, J.H., Gao, J.M., Wang, X.F. and Wu, S.H. (2009). Agglomeration of particles during coal combustion in multistage spouted fluidized tower. *Korean J. Chem. Eng.* 26: 907-912.

Luo, Z., Chen, H., Wang, T., Zhou, D., Lu, M., He, M., Fang, M. and Cen, K. (2017). Agglomeration and capture of fine particles in the coupling effect of pulsed corona discharge and acoustic wave enhanced by spray droplets. *Powder Technol.* 312: 21-28.

Matsoukas, T. (1997). The coagulation rate of charged aerosols in ionized gases. *J. Colloid Interface Sci.* 187: 474-483.

McAdams, R. (2007). Pulsed corona treatment of gases: System scaling and efficiency. *Plasma Sources Sci. Technol.* 16: 703.

O'Hara, D.B., Clements, J.S., Finney, W.C. and Davis, R.H. (1989). Aerosol particle charging by free electrons. J. *Aerosol Sci.* 20: 313-330.

425 Sheng, C. and Shen, X. (2007). Simulation of acoustic agglomeration processes of poly-disperse
426 solid particles. *Aerosol Sci. Technol.* 41: 1-13.
427 Wang, J., Liu, J., Zhang, G., Zhou, J. and Cen, K. (2011). Orthogonal design process
428 optimization and single factor analysis for bimodal acoustic agglomeration. *Powder Technol.*
429 210: 315-322.
430 Wang, Y., Cheng, K., Tian, H.Z., Yi, P. and Xue, Z.G. (2016). Emission characteristics and
431 control prospects of primary pm2.5 from fossil fuel power plants in china. *Aerosol Air Qual.*
432 *Res.* 16: 3290-3301.
433 Xu, F., Luo, Z., Bo, W., Zhao, L., Gao, X., Fang, M. and Cen, K. (2009). Experimental
434 investigation on charging characteristics and penetration efficiency of PM2.5 emitted from coal
435 combustion enhanced by positive corona pulsed esp. J. *Electrostat.* 67: 799-806.
436 Xu, P., Wang, W., Ji, J. and Yao, S. (2014). Analysis of the contribution of the road traffic
437 industry to the PM2.5 emission for different land-use types. *Comput Intell Neurosci.* 2014:
438 821973.
439 Yan, J., Chen, L. and Yang, L. (2016). Combined effect of acoustic agglomeration and vapor
440 condensation on fine particles removal. *Chem. Eng. J.* 290: 319-327.
441 Zhang, G., Zhang, L., Wang, J. and Hu, E. (2017). Improving acoustic agglomeration efficiency
442 by addition of sprayed liquid droplets. *Powder Technol.* 317: 181-188.
443 Zhang, G.X., Liu, J.Z., Wang, J., Zhou, J.H. and Cen, K.F. (2012). Numerical simulation of
444 acoustic wake effect in acoustic agglomeration under Oseen flow condition. *Chin. Sci. Bull.* 57:
445 2404-2412.

Zhou, C.H., Gong, S., Zhang, X.Y., Liu, H.L., Xue, M., Cao, G.L., An, X.Q., Che, H.Z., Zhang, Y.M. and Niu, T. (2012). Towards the improvements of simulating the chemical and optical properties of Chinese aerosols using an online coupled model – CUACE/Aero. *Tellus B Chem Phys Meteorol*. 64: 91-102.

Zhou, D., Luo, Z., Fang, M., Lu, M., Jiang, J., Chen, H. and He, M. (2016a). Numerical calculation of particle movement in sound wave fields and experimental verification through high-speed photography. *Appl. Energy.* 185: 2245-2250.

Zhou, D., Luo, Z., Jiang, J., Chen, H., Lu, M. and Fang, M. (2016b). Experimental study on improving the efficiency of dust removers by using acoustic agglomeration as pretreatment. *Powder Technol.* 289: 52-59.

Table 1. Median particle diameters and agglomeration ratios of particles under various acoustic SPLs and frequencies.

frequency	parameters	SPL		
		135dB	139dB	143dB
800Hz	D_{50}/μm	14.69	24.99	36.88
	R_{ae}	1.84	3.13	4.62
1200Hz	D_{50}/μm	18.76	27.22	36.95
	R_{ae}	2.35	3.41	4.63
1600Hz	D_{50}/μm	28.50	41.27	57.56
	R_{ae}	3.57	5.17	7.21
2000Hz	D_{50}/μm	23.15	26.10	28.10
	R_{ae}	2.90	3.27	3.52
2400Hz	D_{50}/μm	9.50	15.97	20.52
	R_{ae}	1.19	2.00	2.57

Figure Captions

Fig. 1. Schematic of experimental setup.

Fig. 2. Relationship between the entrainment factor and particle diameter at various acoustic frequencies.

Fig. 3. Original particle size distribution of the ash.

Fig. 4. Influence of the input voltage on the single pulse energy of pulse corona discharge.

Fig. 5. Volume differential (a) and cumulative distribution (b) of particle size under various pulse input voltages and frequencies.

Fig. 6. Median particle diameters and agglomeration ratios of particles under various pulse input voltages and frequencies.

Fig. 7. Volume differential (a) and cumulative distribution (b) of particle size under various acoustic wave frequencies (SPL = 143 dB).

Fig. 8. Median particle diameters and agglomeration ratios of particles under various acoustic wave frequencies (SPL = 143 dB).

Fig. 9. Volume differential (a) and cumulative distribution (b) of particle size under single field and coupling field.

Fig. 10. Comparison of particle number distribution after ESP under various pretreatment conditions.

Fig. 11. Grade removal efficiency of fine particles after application of ESP with single field and coupling field.

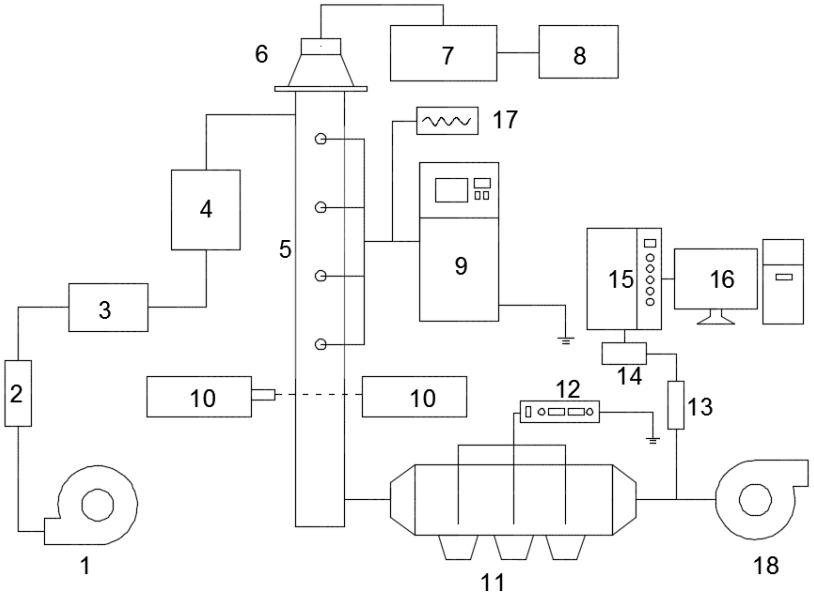

1.Blower 2.flowmeter 3.feeding system 4.buffer tank 5.agglomeration chamber 6.compression driver 7.power amplifier 8.signal generator 9.narrow-pulse high-voltage generator 10.DP-02 laser particle analyzer 11.ESP 12.high voltage DC power supply 13.electrostatic neutralizer 14.diluter 15.ELPI 16.computer 17.oscilloscope 18.vacuum pump

Fig. 1. Schematic of experimental setup.

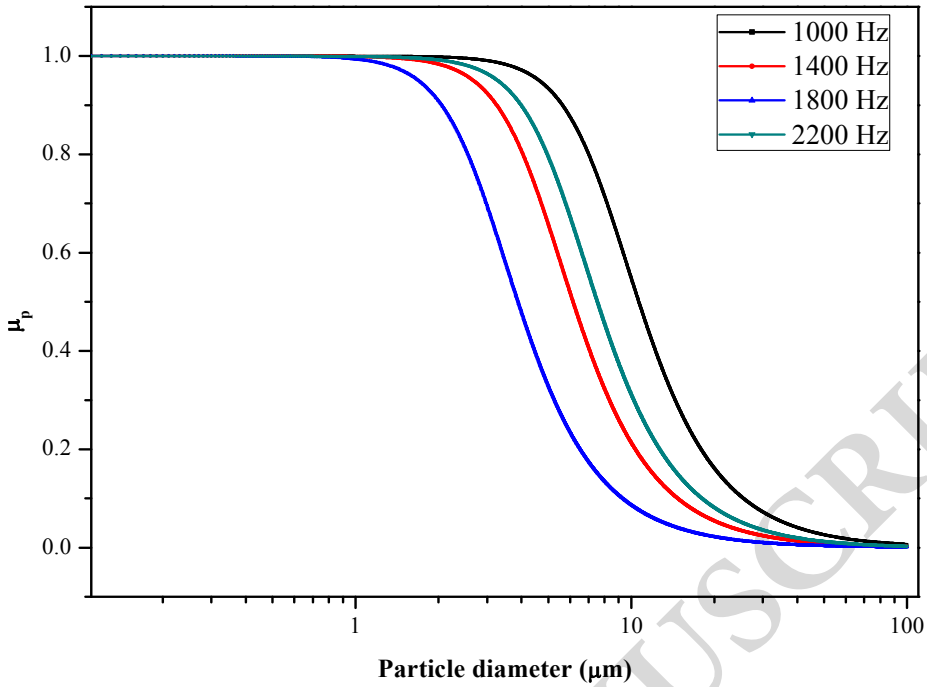

517

518 **Fig. 2.** Relationship between the entrainment factor and particle diameter at various acoustic

519 frequencies.

520

521

522

523

524

525

526

527

528

529

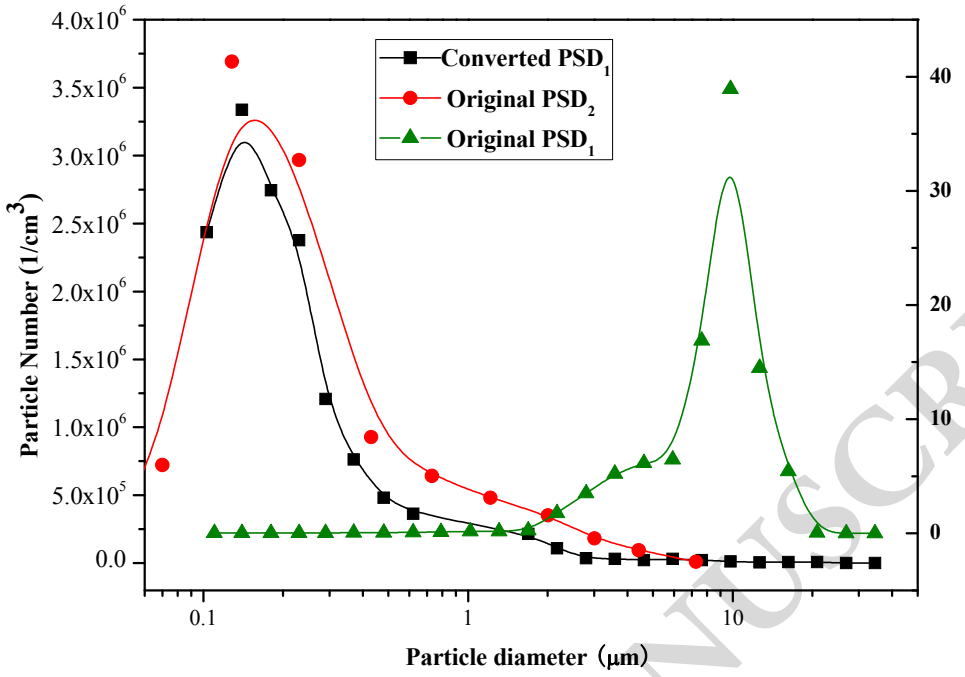

530

531 **Fig. 3.** Original particle size distribution of the ash.

532

533

534

535

536

537

538

539

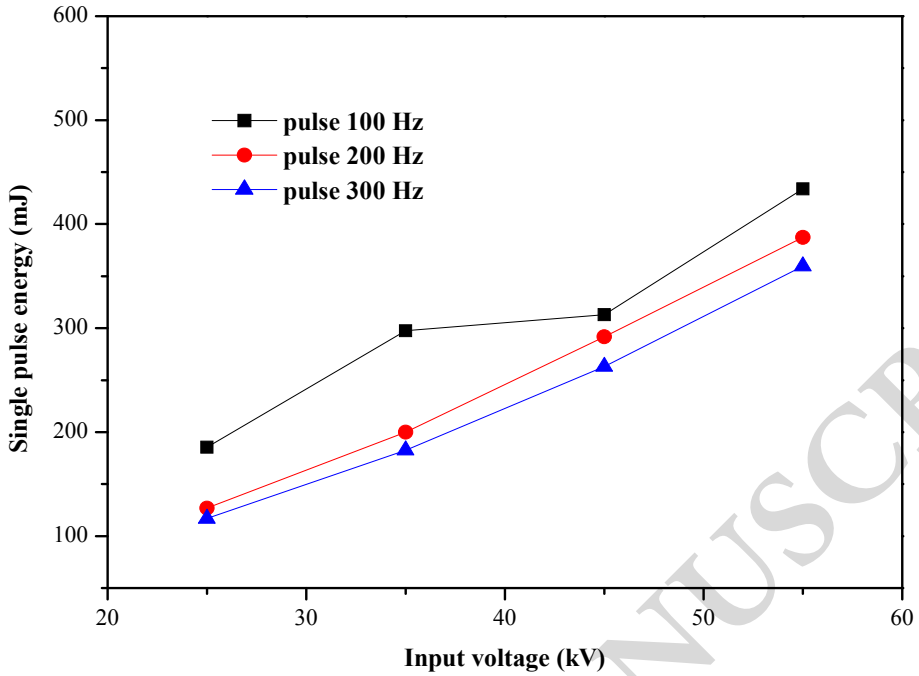

Fig. 4. Influence of the input voltage on the single pulse energy of pulse corona discharge.

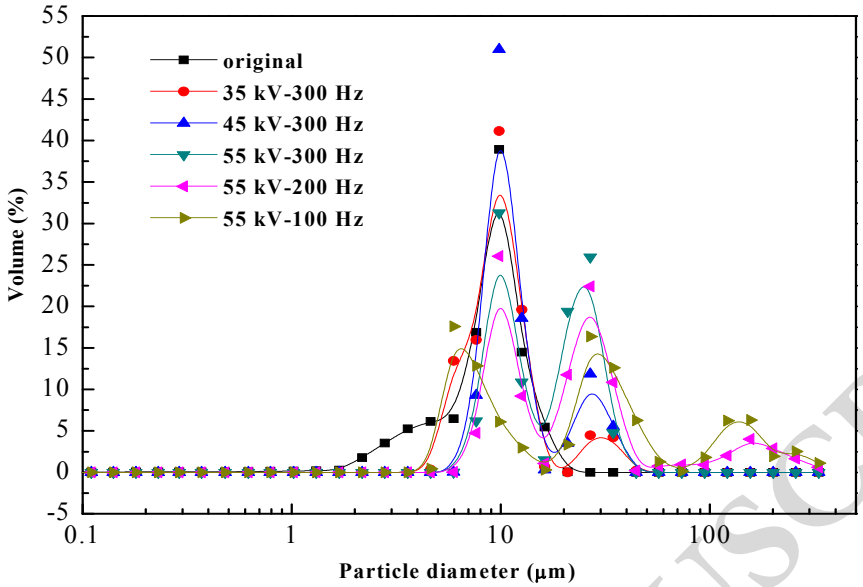

552

553 **(a)**

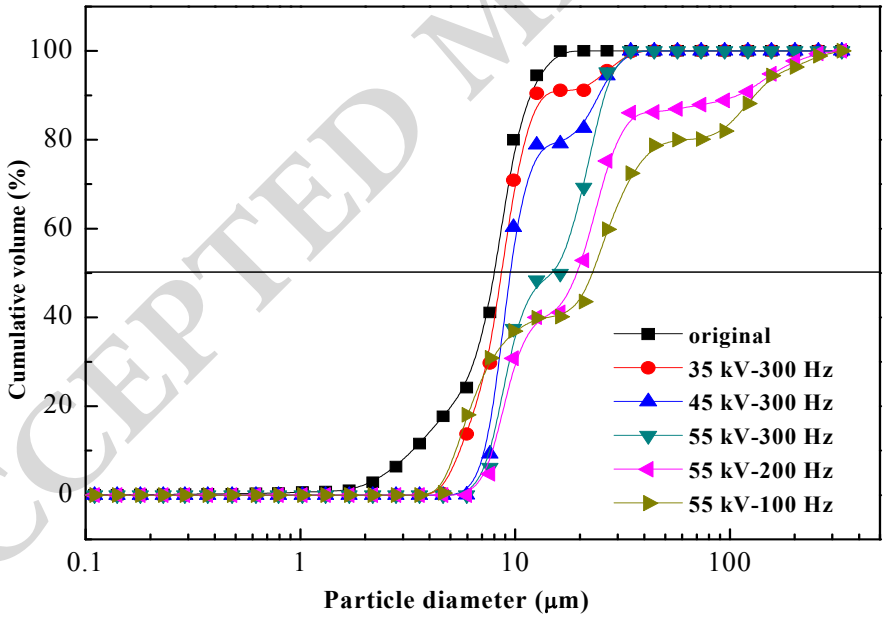

554

555 **(b)**

556 **Fig. 5.** Volume differential (a) and cumulative distribution (b) of particle size under various pulse

557 input voltages and frequencies.

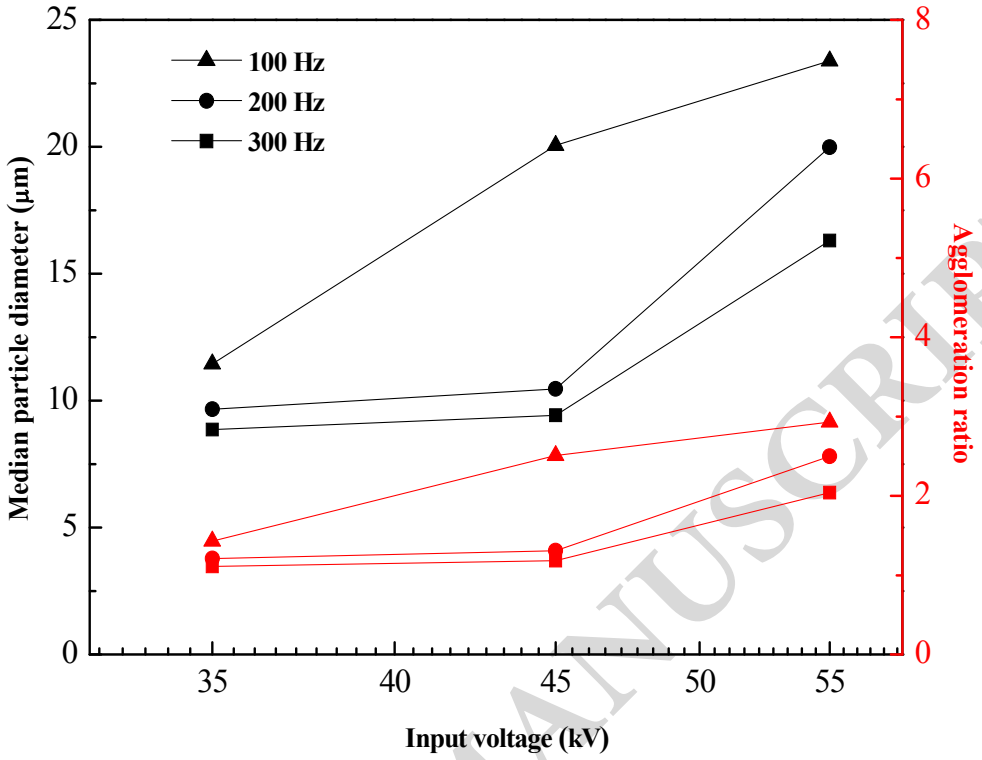

Fig. 6. Median particle diameters and agglomeration ratios of particles under various pulse input voltages and frequencies.

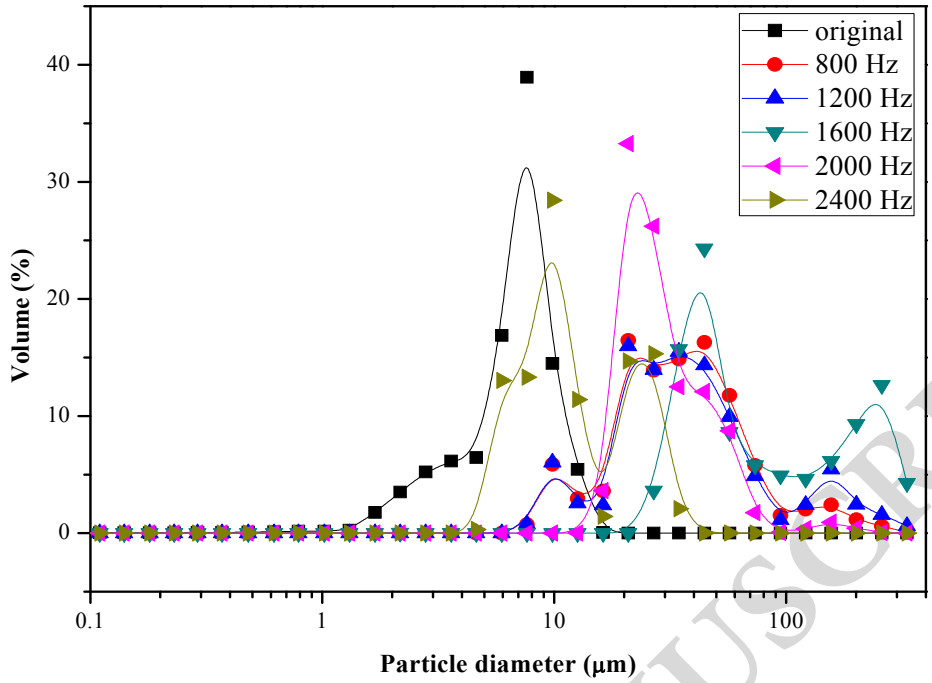

569

570 **(a)**

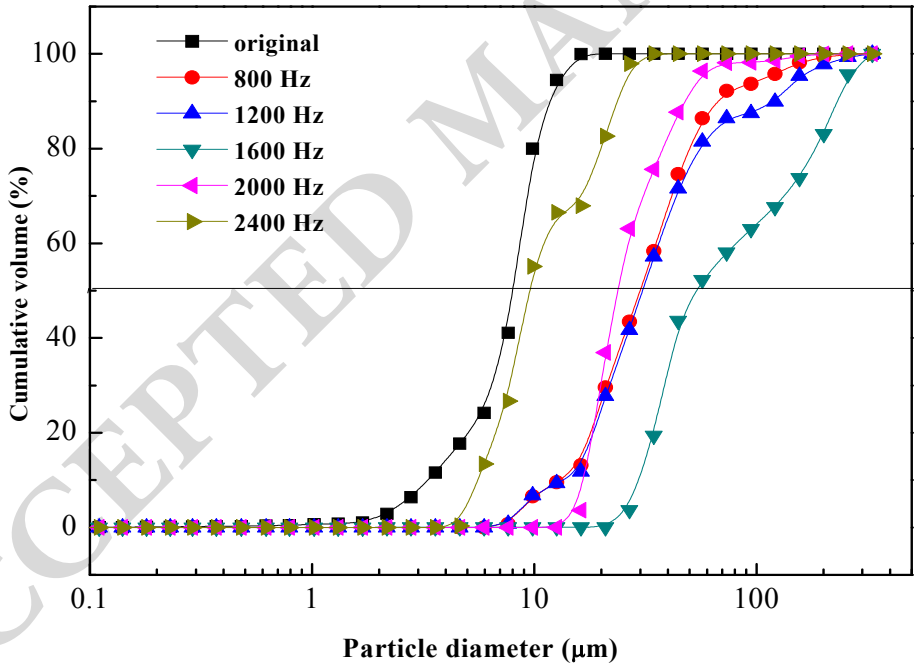

571

572 **(b)**

573 **Fig. 7.** Volume differential (a) and cumulative distribution (b) under various acoustic wave

574 frequencies (SPL = 143 dB).

575

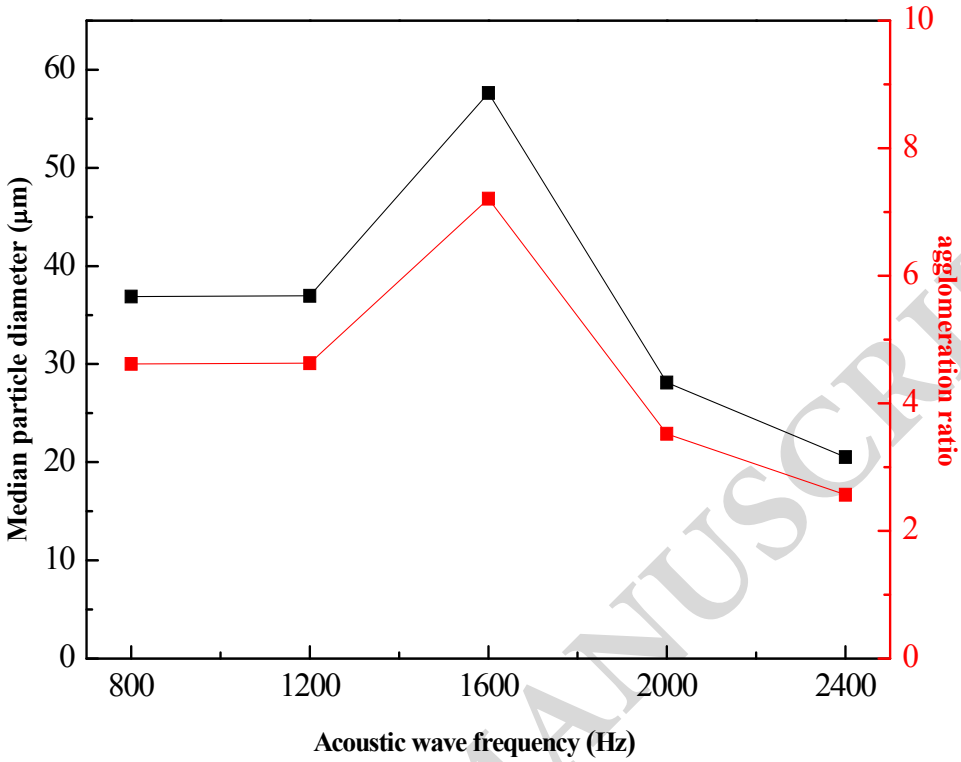

Fig. 8. Median particle diameters and agglomeration ratios of particles under various acoustic wave frequencies (SPL = 143 dB).

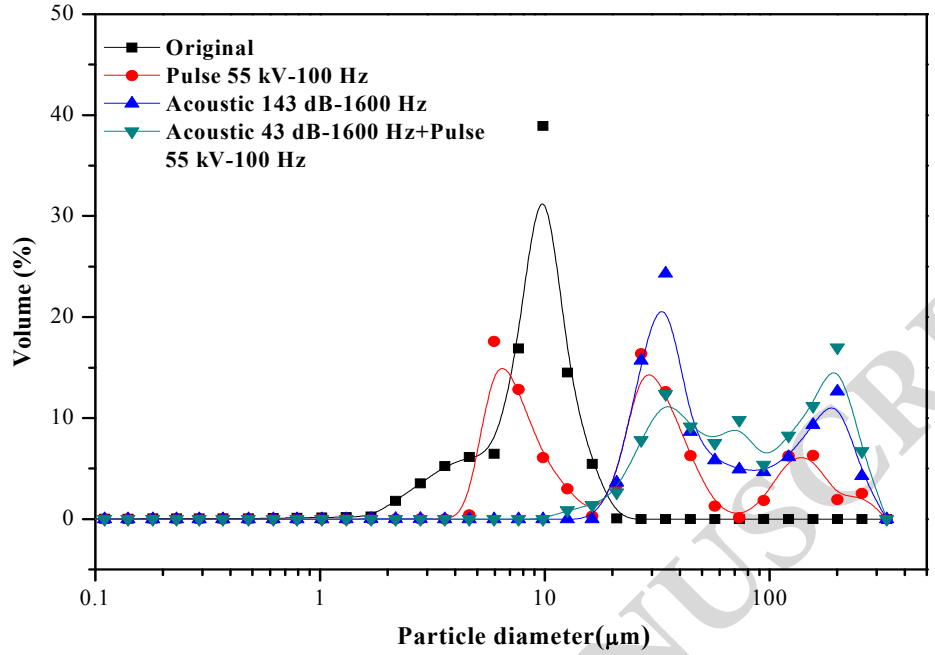

(a)

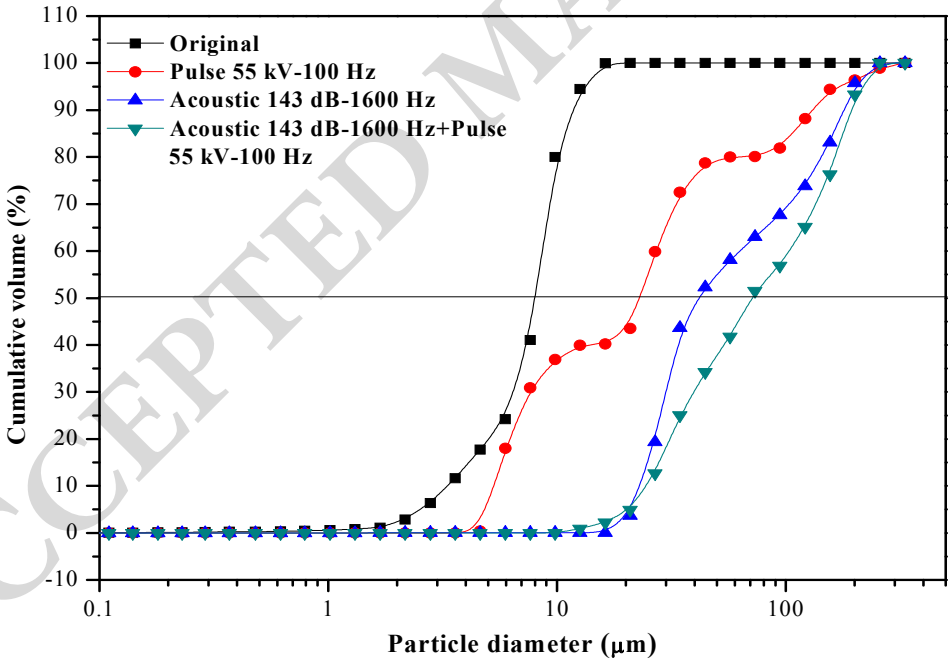

(b)

Fig. 9. Volume differential (a) and cumulative distribution (b) of particle size under single field and coupling field.

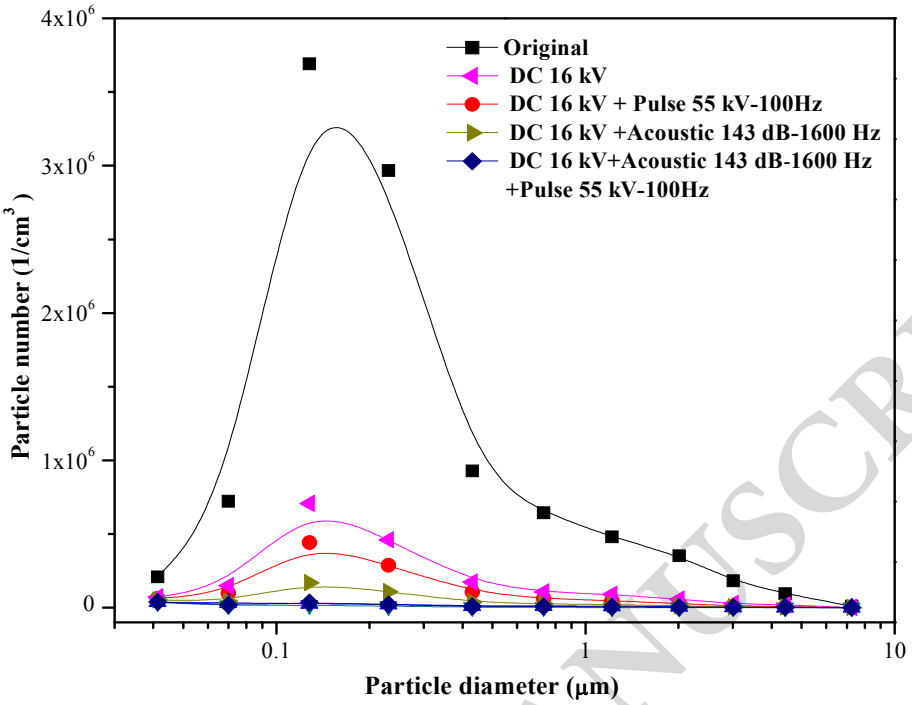

Fig. 10. Comparison of particle number distribution after ESP under various pretreatment conditions.

610

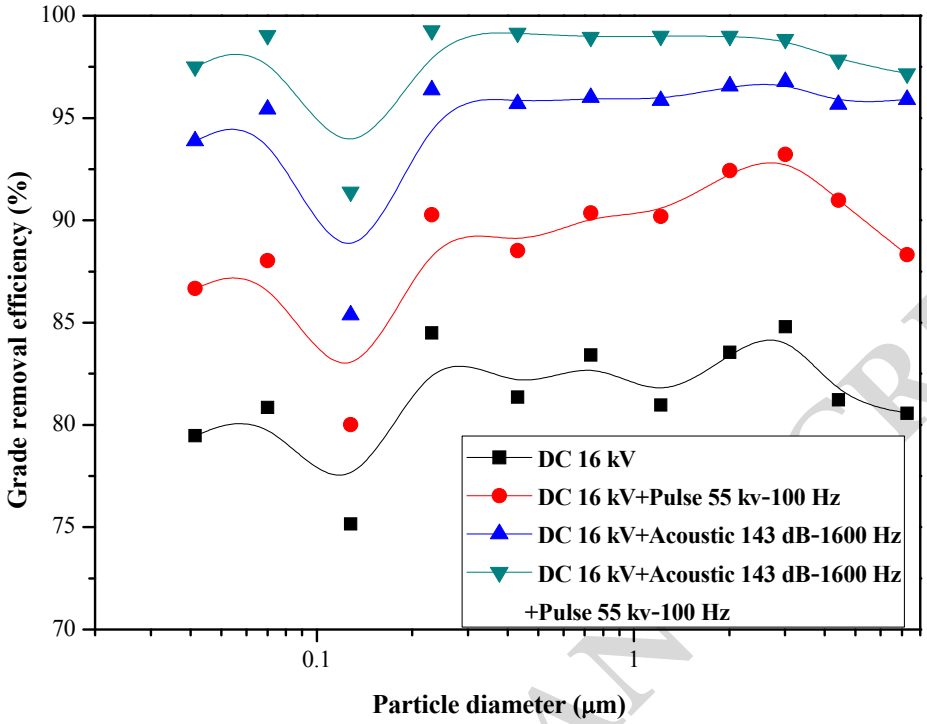

611

612 **Fig. 11.** Grade removal efficiency of fine particles after application of ESP with single field and

613 coupling field.

614